

Three-Dimensional Structural Behavior of the Bitter Plate Toroidal Field Magnet for the ZEPHYR Ignition Test Reactor

E.S. Bobrov, J.E.C. Williams

*Plasma Fusion Center,
Massachusetts Institute of Technology, Cambridge, Massachusetts 02139, U.S.A.*

Computer structural analyses of a Bitter plate Ignition Test Reactor Toroidal Field (ITR TF) magnet are discussed in this paper. Several finite element (FE) models were generated for the purpose of these analyses.

An interactive computer code which incorporates the ANSYS finite element analysis program has been developed at MIT. The code generates a sequence of solutions which includes a steady-state or a transient electrical conductivity analysis, magnetic field analysis, generation of Lorentz body forces, and finally, stress and displacement analysis.

The three-dimensional FE model takes into account the laminated character of the wedge-shaped plates. Each plate is made of bonded copper and stainless steel and is separated from adjacent plates by G-10 insulation. The model takes into account singularities in geometry and in structural and electrical material properties caused by the presence of the neutral beam and diagnostic ports and cranked turns. Relative sliding of the plates due to poloidal field loads is taken into account, too. A detailed variation of stresses and displacements with respect to the three coordinates is presented and discussed. Special attention is given to the stress concentrations around the neutral beam ports and areas with sudden changes of material physical properties.

These results are compared with results obtained from the single plate FE model.

1. Introduction

Methods and results of computer structural analyses of the Bitter plate ZEPHYR Ignition Test Reactor Toroidal Field magnet [1] are discussed in this paper. Several discrete models were generated for the purpose of these analyses.

Two principal in plane loads acting on the TF coil are taken into account.

1. In plane Lorentz forces induced by the toroidal field
2. Radial surface pressure produced by the girth rings/poloidal coils

The analysis of the structural behavior of the TF magnet subject to the two loads was performed on the basis of the finite element method, for which two computer models have been generated. The first model did not take into account the geometric singularities caused by the presence of the neutral beam and diagnostic ports, and treated the magnet as consisting of 256 identical laminated (copper-steel-insulation) wedged plates. Each of these plates was considered to have two planes of symmetry, RZ and R θ , which are shown in Figure 1. This allows one quadrant only of the laminated plate to be modeled.

A special interactive computer code which incorporates the ANSYS [2] finite element analysis program has been developed. The code generates a sequence of solutions which include a steady-state or a transient electrical conductivity analysis (but excluding magnetic diffusion), magnetic field analysis, generation of Lorentz body forces, and finally, stress and displacement analysis.

The second FE model developed on the basis of the former was closer to the three-dimensional reality. The major goal pursued and achieved by this model was to find the variation of stresses and displacements with respect to the circumferential coordinate and to account for the presence of the neutral beam ports. The model represented the upper half of a 22.5° wedge (Figure 2) bounded by two radial toroidal planes of symmetry and one central plane normal to the vertical axis, thus only half of the coil extending 22.5° from the diagnostic port midplane was considered.

2. Single-Plate Axisymmetric Model of the TF Magnet

2.1 General Characteristics of the Model

This model represents one quadrant of a laminated Bitter plate. Its analysis gives a detailed picture of the TF magnet structural behavior if the singularities caused by the neutral beam (NB) ports are neglected. As will be demonstrated later this model generates an accurate picture of stresses and displacements away from the NB ports. This especially relates to the throat region where the vertical, radial, and circumferential stresses seem to be least affected by the presence of the ports.

The plate is defined in cylindrical coordinates with a radial coordinate R measured from the central axis of the magnet system, a vertical coordinate Z measured from the horizontal plane of symmetry, and an angle θ measured from the vertical plane of symmetry of the thickness of the laminated plate. The coordinate axes and the principal dimensions which serve as input data for the FE model generation are shown in Figure 3.

The wedge plate is composed of a copper current-carrying central section (a symmetric turn is considered), a steel load carrying plate bonded to copper, and a layer of insulation separating the plate from an adjacent wedge. Because of symmetry, the insulation thickness in the model equals half of the actual insulation thickness.

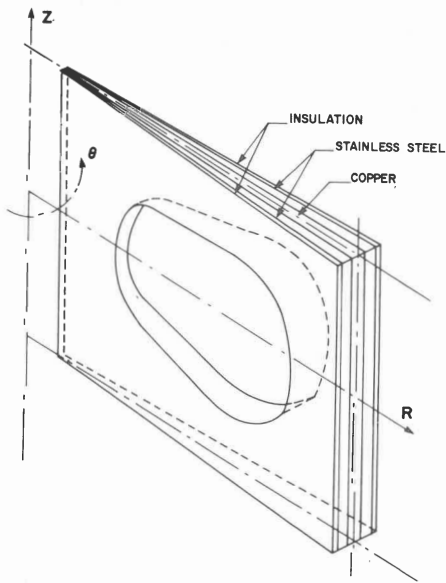


Figure 1. Laminated Bitter Plate Considered in the Single-Plate Analysis

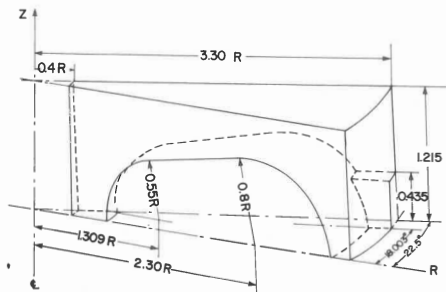


Figure 2. A 22.5°-Wedge Model with the Neutral Beam Port Window

In accordance with the data describing the geometry of the coil and with the precision of the finite element grid in each specified region of the plate, the program automatically generates the grid point mesh. Each of the three materials is represented by one layer of finite elements in the circumferential direction. No constraint is imposed on the fineness of the mesh in the RZ plane.

After the mesh generation is completed a steady-state or a transient current density distribution analysis is performed. For this purpose three-dimensional isoparametric solid electrical finite elements with 8 nodal points (one degree of freedom in each - the potentials) are used. Geometrically they are identical with the finite elements used in the stress and displacement analysis. The output of this part of the code includes voltages and current components at the nodal points as well as the current densities at the centroids of the elements. On the basis of the current distribution the magnetic field analysis is conducted.

The next step is generation of the Lorentz forces which are later converted into the surface pressures acting on the sides of the finite elements. These pressures along with the pressures applied to the boundaries of the coil (for example, the radial compression from the girth-rings) are the input data for the FEM stress analysis.

Three-dimensional isoparametric solid elements with eight nodal points and 24 degrees of freedom (nodal linear displacements) represent copper and steel. The insulation is modeled with three-dimensional interface elements which are capable of supporting only compressive stresses in the circumferential direction and limited shear stresses in the RZ plane. This means that when the shear exceeds the friction, slip occurs.

The following elastic moduli of the structural materials were used in this analysis:

- | | |
|--------------------|-------------------------------|
| 1. Copper | - 137.9 GPa in all directions |
| 2. Stainless Steel | - 206.8 GPa in all directions |
| 3. G-10 Insulation | - 27.6 GPa in all directions |

A Poisson's ratio of 0.3 was used for all three materials. The coefficient of friction between G-10 insulation and stainless-steel was assumed to be 0.3 to account for any possible slippage.

2.2 Stress and Displacements Due to the TF Field

Stresses and displacements under the action of in plane Lorentz forces were generated by this model at an operating current of 246 kA. Both in copper and steel the maximum tensile stresses take place in the throat region and are 298 MPa and 466 MPa, respectively. The maximum radial tensions occur approximately in the middle of the upper and lower arms, at the edges. They are 79.2 MPa and 119 MPa, in the copper and steel plates, respectively. The arms of the coil experience substantial bending. The maximum horizontal shear stress $\tau_{R\theta}$ (2 MPa) between copper and steel takes place in the throat region, at the midplane.

The circumferential stress distribution due to the Lorentz forces is important from the point of view of the contribution of the Lorentz force to the frictional shear necessary to withstand the overturning forces induced by the poloidal field. The maximum compression of 151 MPa takes place at the inner edge of the throat near the horizontal midplane. In the outer corner region the σ_{θ} compressive stresses induced by toroidal field Lorentz forces are negligible. For this reason precompression by means of girth-rings is used.

The maximum inward radial displacement of 0.96 mm due to the in plane Lorentz forces is experienced by the throat region at the horizontal midplane. The maximum vertical displacement of 1.67 mm takes place at the inner boundaries of upper and lower arms of the coil.

2.3 Stresses and Displacements Due to Precompression

In order to compensate for the lack of circumferential compression in the outer limb region which is needed to provide frictional shear against the overturning force, the TF magnet is precompressed after assembly by means of girth rings (PF coils). The radial clamping pressure exerted on the toroidal magnet over a height of 0.5 m at the upper and lower outer corners of the plates is 37.9 MPa.

The additional circumferential compression generated by the precompression load in the outer limb region varies from 14.6 MPa at the midplane to 37.3 MPa at the upper and lower outer corners of the coil.

In the throat region, the vertical (σ_z) precompression stresses in copper and steel are compressive. This leads to the reduction of the σ_z stresses generated in the region by in plane Lorentz forces.

The comparison of the displacement profiles caused by each of the inplane loads leads

to the conclusion that when the operating current achieves its nominal value the poloidal coils will follow the torus without separation, and that the precompression which provides additional frictional shear in the vulnerable outer limb region will be maintained.

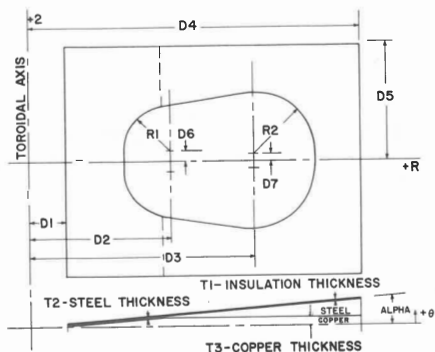


Figure 3. Wedge-Conductor Plate Geometry

3. A 22.5° Wedge FEM Model of the TF Magnet With NB Ports

3.1 Description of the Model

As has been emphasized earlier in this paper, the single-plate model of the TF magnet introduces certain simplifications. In particular, it does not reveal the peculiarities in the structural behavior of the magnet caused by the presence of the neutral beam ports. This especially relates to the circumferential stress distribution in the vicinity of the port boundaries. A three-dimensional 22.5° model of the TF Bitter plate magnet with 8 neutral beam ports (the torus has 16 planes of mirror symmetry) has been generated for the purpose of the detailed analysis.

The FEM wedge model was developed in a relatively short time because the most time consuming procedures for this model were acquired from the interactive code for the single-plate model. This relates especially to the automatic mesh generation in the vertical radial planes, to the current density and field analyses, and to the generation of the Lorentz body forces.

The general view of the section representing 1/32 of the TF magnet structure, is shown in Figure 2. A simplification relating to the orientation of the central axis of the neutral beam port is used in the model. In the model the axis of the beam line is perpendicular to the plasma axis while in the actual magnet it is angled by about 20°.

Figure 4 presents an isometric view of the FEM mesh generated for the analysis. In the circumferential direction the wedge is represented by 9 sectors. The angles subtended by these sectors are not equal. This is done in order to follow as closely as possible the variations in the geometry, the Lorentz body forces, and the material properties with respect to the circumferential coordinate.

Each of the 9 sectors is modeled by 112 three-dimensional isoparametric solid elements of the ANSYS type. The FEM mesh in the RZ planes of the model generated for this analysis is shown in Figure 5. The model has 3815 degrees of freedom. In order to avoid complications associated with the laminated structure of the Bitter plates (copper, steel,

insulation) a special homogenization technique was used. Except for the small area in sectors 5 and 6 adjacent to the port where the cranked turns are located, elements whose centroids have the same coordinates in the RZ planes were assumed to have constant elastic properties with respect to the circumferential coordinate.

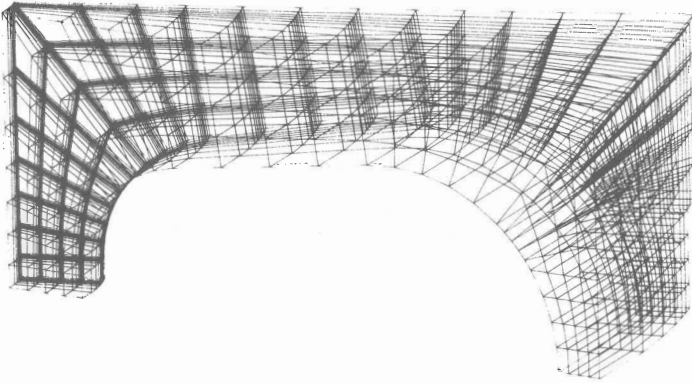


Figure 4. Three-Dimensional FEM Model

In accordance with the variation of the relative fractions of copper, steel, and insulation in the plate cross-section as a function of its radial coordinate (nonsymmetric wedge) as shown in Figure 6, anisotropic compound properties of finite elements at various radial locations were computed. Thirty-five material combinations including a material with zero stiffness in the port region, were used for the finite elements in this analysis. The source properties of copper, steel, and insulation were the same as in the single-plate model. Associated with the material types were the relative current densities. This takes into account the increased current densities in the cranked turns.

The Lorentz forces were first calculated on the basis of the single-plate model, after which, for all radii and vertical levels at which the nodal points are located, the linear load per unit angle was found. The nodal forces and face pressures were then computed in accordance with the angles subtended by respective elements in their sectors.

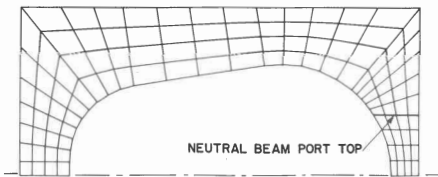


Figure 5. Finite Element Mesh in RZ-planes

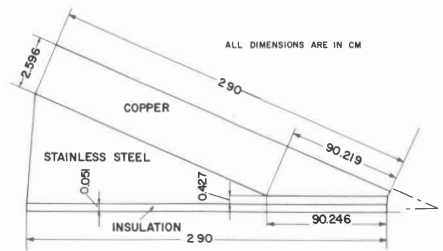


Figure 6. Nonsymmetric Wedge Cross-Section

3.2 Discussion of the Analytical Results

The results of the three-dimensional FEM analysis of the TF magnet subject to in plane

Lorentz forces and precompression are illustrated in Figures 7 through 23 in the form of equal stress lines and deformed shapes of the plates in various cross-sections. All stresses are given in MPa averaged over the compound material.

Figures 7 and 8 show the distribution of the vertical axial stresses σ_z in cross-sections coinciding with the two vertical planes of symmetry in the torus. It is pointed out that the pattern of the σ_z stress distribution in the throat region is exactly the same in all nine angular cross-sections. This means that the singularity caused by the presence of the port in the outer limb does not affect the vertical stresses in the throat region. In the outer limb region between the symmetry plane $\theta = 0$ and the side of the port, there is a noticeable variation of the σ_z - stress pattern. Although the magnitudes of the stress above the port are small there is a variation of the σ_z - stress distribution with respect to the angular coordinate.

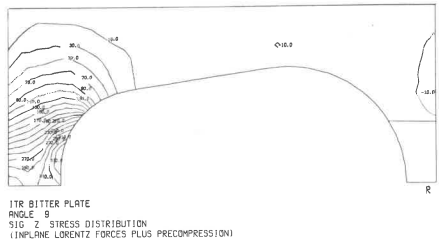
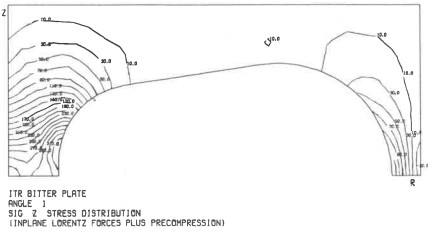


Figure 7. σ_z -Stress Distribution in the $\theta = 0$ Plane (Middle Between Ports)

Figure 8. σ_z -Stress Distribution in the $\theta = 22.5^\circ$ (Port Midplane)

Figures 9, 10, and 11 present the distribution of the circumferential stress, σ_θ , in various cross-sections. In the throat and horizontal arm regions the patterns of the stress distribution in all 9 cross-sections look almost identical. However, in the outer limb area there is an apparent variation in stress values and the pattern of its distribution with respect to the angular coordinate. In the cross-sections which are very close to the side of the port which is a stress-free surface, the circumferential stress almost disappears while a stress concentration can be observed above the port (Figure 9). Directly above the port the stress concentration becomes stronger with maximum values of about 140 MPa, as shown in Figure 10.

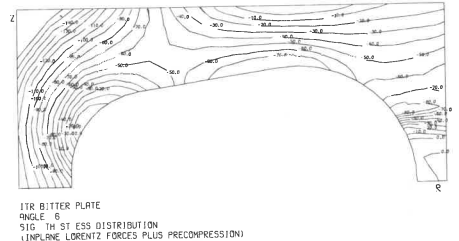
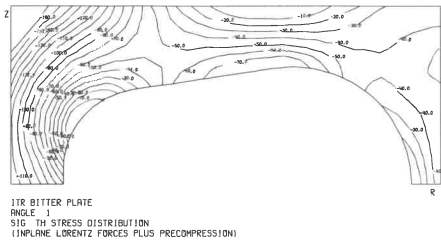


Figure 9. σ_θ -Stress Distribution in the $\theta = 0$ Plane

Figure 10. σ_θ -Stress Distribution Near the Port Side

The radial stresses are illustrated in Figures 12 and 13. In the throat and in most of the top and bottom horizontal arm regions there is again almost no variation in the stress pattern with respect to the angular position of the cross-section. In all cross-sections the distribution of the σ_R - stress shows that the horizontal arm is a beam in bending. The nonzero radial stresses on the outer surface of the torus are due to the radial pressure from the girth-rings.

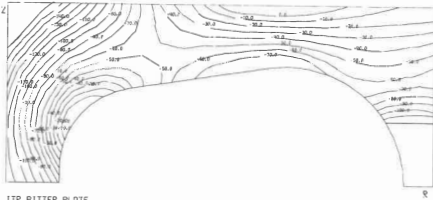


Figure 11. σ_θ -Stress Distribution in the $\theta = 22.5^\circ$ Plane

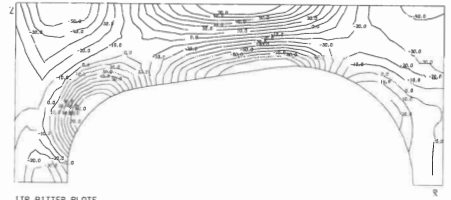


Figure 12. σ_R -Stress Distribution in the $\theta = 0^\circ$ Plane

Figures 14 through 16 illustrate the distribution of the shear stress, $\tau_{\theta Z}$, in the wedge. The pattern of the distribution of these stresses and their values and signs vary substantially with respect to the angular coordinate. In the throat region and the inner half of the horizontal arm the shear stresses change their signs between the sides of the wedge. In the vicinity of the port side in the outer limb region a strong shear stress concentration takes place at the top of the port. Directly above the port the shear stress decreases rapidly.

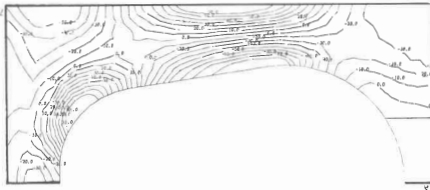


Figure 13. σ_R -Stress Distribution in the $\theta = 22.5^\circ$ Plane

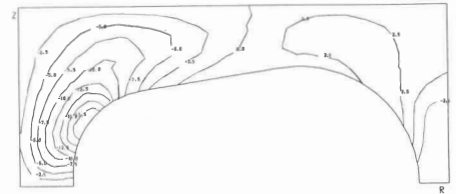


Figure 14. $\tau_{\theta Z}$ -Stress Distribution Close to the $\theta = 0^\circ$ Plane

The horizontal shear stresses, $\tau_{R\theta}$, acting in the vertical radial cross-sections are shown in Figures 17 through 19. As in the previous case these stresses vary substantially with respect to θ , and change signs in the entire cross-section between the left side of the wedge and the port side.

As can be seen in Figures 20 and 21 the τ_{RZ} shear stresses are almost independent of the θ -coordinate. There is a strong concentration of this shear stress in the throat region

where it reaches a value of almost 130 MPa.

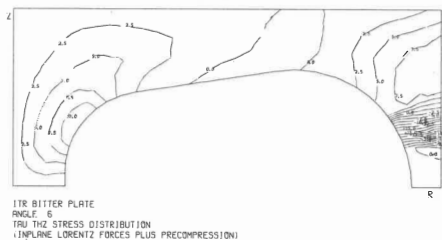


Figure 15. $\tau_{\theta Z}$ -Stress Distribution Near the Port Side

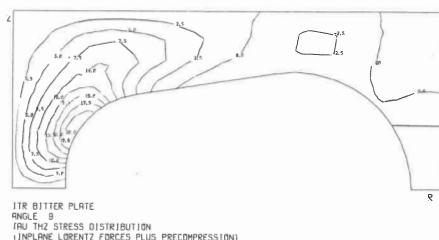


Figure 16. $\tau_{\theta Z}$ -Stress Distribution in the Vicinity of the Port Midplane

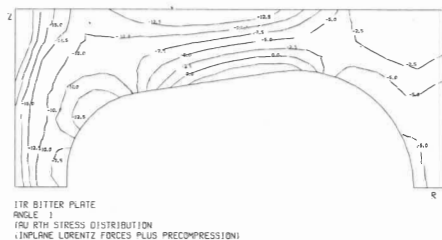


Figure 17. $\tau_{R\theta}$ -Stress Distribution Close to $\theta = 0$ Plane

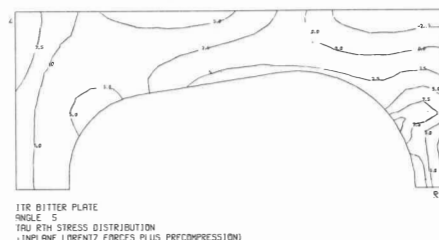


Figure 18. $\tau_{R\theta}$ -Stress Distribution Near the Port Side

Figures 22 and 23 illustrate the in plane displacements of the TF coil contours in the 22.5° wedge model. Figure 22 shows the deformed shapes of the coil at the symmetry plane $\theta = 0$ under the in plane loads (Lorentz forces, precompression). Under the action of Lorentz forces the maximum inward radial displacement of 1.235 mm takes place in the outer limb at the horizontal plane, $Z = 0$. The maximum vertical displacement of 2.246 mm was forced to occur approximately in the middle of the horizontal arms at the inner contour.

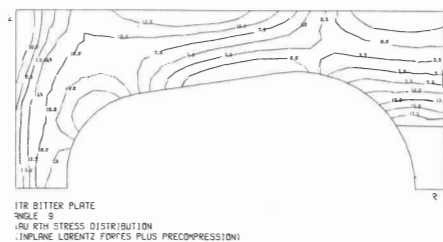


Figure 19. $\tau_{R\theta}$ -Stress Distribution in the Vicinity of $\theta = 22.5^\circ$ Plane

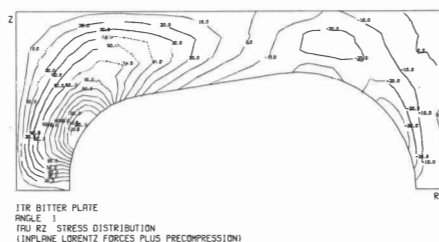


Figure 20. τ_{RZ} -Stress Distribution in the Vicinity of $\theta = 0$ Plane

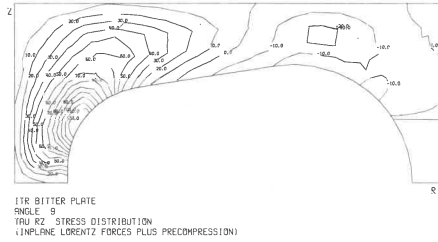


Figure 21. τ_{RZ} -Stress Distribution in the Vicinity of the $\theta = 22.5^\circ$ Plane

Figure 22 also shows the deformed shape of the coil cross-section under the combined action of in plane Lorentz forces and precompression. This is compared with the underformed shape of the coil. The maximum resulting horizontal (1.694 mm) and vertical (2.388 mm) displacements are experienced by the same points of the coil boundary as in the case of loading by pure Lorentz forces.

Figure 23 shows the superposition of the deformed shapes of the magnet cross-sections at $\theta = 0$ and $\theta = 22.5^\circ$, center of the port, both under the cumulative action of in plane Lorentz forces and radial precompression. The two deformed shapes evidently do not differ much in most regions of the contour away from the immediate vicinity of the port. The major difference which is rather small takes place quite close to the port and mostly affects the vertical displacements.

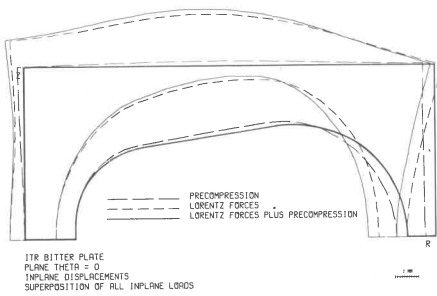


Figure 22. Superposition of In Plane Displacements Caused by Two Loads and Their Combination

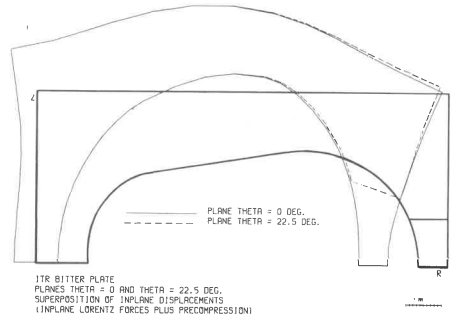


Figure 23. Superposition of In Plane Displacements of Both Planes of Symmetry of the Model

4. Conclusion

The structural details and dimensions used in the FEM analyses of both the single-plate and the 22.5° wedge models relate to early versions of the Bitter plate TF magnet design. They are different from those used in the final version of the design described in [3].

However, the results of the analyses presented in this section and of several preliminary and intermediate analyses lead to the conclusion that qualitatively and to a certain degree, quantitatively, the described results are applicable to the present design.

This applies especially to the throat region where the magnitudes of the stresses and the patterns of stress distribution are least affected by variations in the outer radius of the torus and by the presence of geometric and material singularities in the outer limb region.

Comparison of results generated by the single-plate and 22.5° wedge models indicates that the sophisticated three-dimensional analysis generates refined stress and displacement data only in the vicinity of the ports while the rest of the magnet structure is only slightly influenced by the presence of the ports. This is especially clear when the deformed shapes of the magnet cross-sections at different angular positions are compared, as shown in Figure 23.

The single-plate laminated model which is cheaper and simpler to compute is adequate, both qualitatively and quantitatively for all regions except those close to the port. It can be used as a reliable analytical tool during all major stages of design.

The three-dimensional model is capable of generating a detailed picture of magnet structural behavior in all regions. It is appropriate to the final design stage when dimensions and structural details of the system are already established.

5. Acknowledgements

This work was supported by the Fusion Energy Branch of the U.S. Department of Energy.

The authors wish to acknowledge the contribution of F. Everett Reed and Suzanne Stitt (Littleton Research and Engineering Corp.), Michael Weinreich (independent consultant) and Dorette Sarachik (MIT).

References

- [1] H. Becker, E. S. Bobrov, L. Bromberg, D. Cohn, J. M. Davin, J. E. C. Williams, A Toroidal Bitter Plate Magnet for an Ignition Test Reactor, Presented at the 11th Symposium on Fusion Technology, Oxford, England, September, 1980.
- [2] G. J. DeSalvo and J. A. Swanson, ANSYS Engineering Analysis System, User's Manual, Swanson Analysis Systems, Inc., Houston, Pennsylvania, 1978.
- [3] J. E. C. Williams, D. Cohn, H. Becker, E. S. Bobrov, L. Bromberg, J. M. Davin, The Conceptual Design of a Bitter Plate Toroidal Field System for an Ignition Test Reactor, MIT Plasma Fusion Center Report, U.S. DOE Contract DE-AC02-77 ET 52021, Cambridge, Massachusetts, 1981.

